**Supplementary Figure 1**

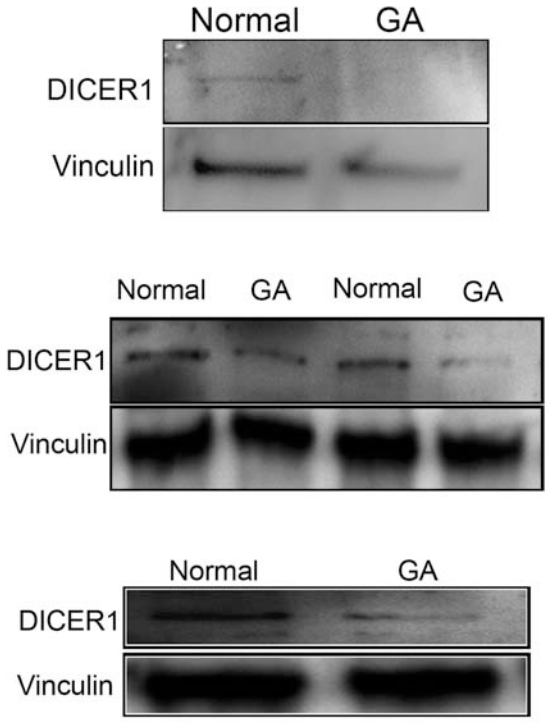


**DICER1 levels in RPE are reduced in geographic atrophy.** Western blots of macular RPE lysates from individual human donor eyes show that DICER1 protein abundance, normalized to the levels of the housekeeping protein Vinculin, are reduced in geographic atrophy (GA) compared to age-similar control human eyes without age-related macular degeneration.

**Supplementary Figure 2**

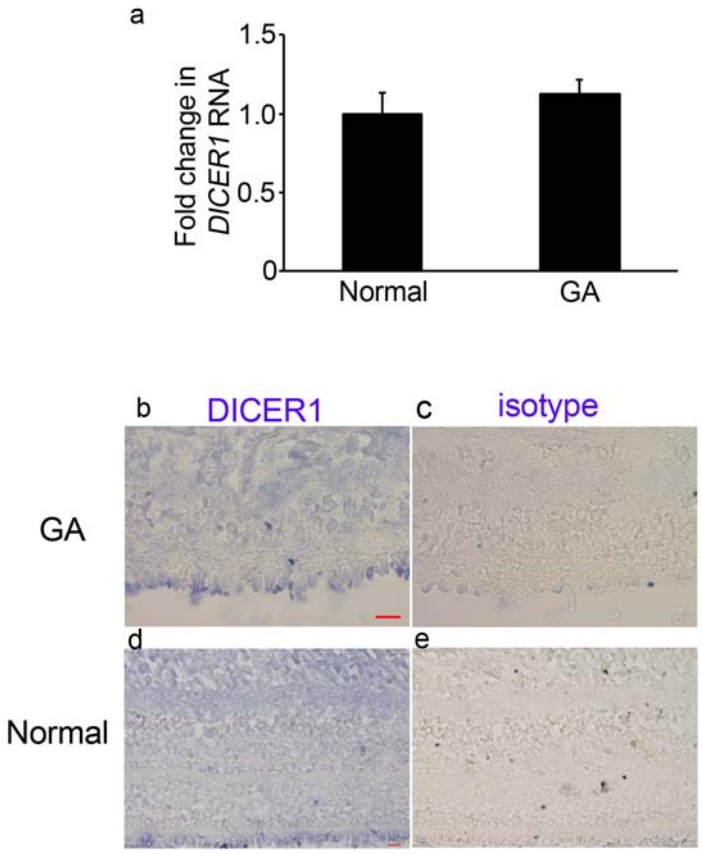


**DICER1 levels in neural retina are unchanged in geographic atrophy. a,** *DICER1* mRNA abundance in the neural retina, as monitored by real-time RT-PCR, was not significantly different ($P > 0.05$ by Mann Whitney U test) between normal human retinas and those with geographic atrophy. Levels normalized to 18S rRNA abundance and to normal retinas. n=7. **b–e,** DICER1 protein immunolocalization in the neural retina was not different between human eyes with geographic atrophy (**b**) and normal (**d**) eyes. Specificity of DICER1 staining was confirmed by absence of reaction production with isotype control antibody (**c,e**). Representative images shown. n=8. Scale bars (20 μm, **b–e**).

**Supplementary Figure 3**

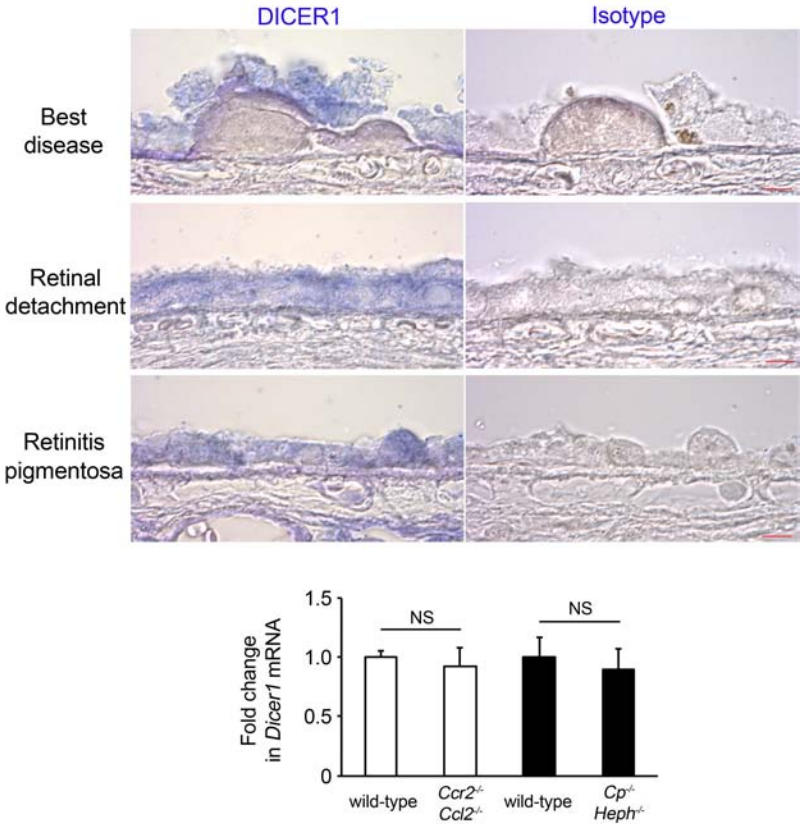


**DICER1 is not generically downregulated in retinal diseases.** Immunolocalization studies revealed abundant DICER1 protein expression (blue, left column) in the RPE in the eye of an 85-year-old man with Best disease (vitelliform macular dystrophy), a 68-year-old man with retinal detachment secondary to choroidal melanoma, and a 72-year-old woman with retinitis pigmentosa. Specificity of DICER1 staining was confirmed by absence of reaction production with isotype control antibody (right column). Representative images shown. n=13. Scale bars (10 μm). *Dicer1* mRNA expression in the RPE was not significantly (NS) different in *Ccl2*$^{-/-}$ *Ccr2*$^{-/-}$ mice or *Cp*$^{-/-}$ *Heph*$^{-/-}$ mice compared to their background strains. Transcript abundance quantified by real-time RT-PCR and normalized to 18S rRNA and to control eye levels. n=6. NS, not significant.

**Supplementary Figure 4**

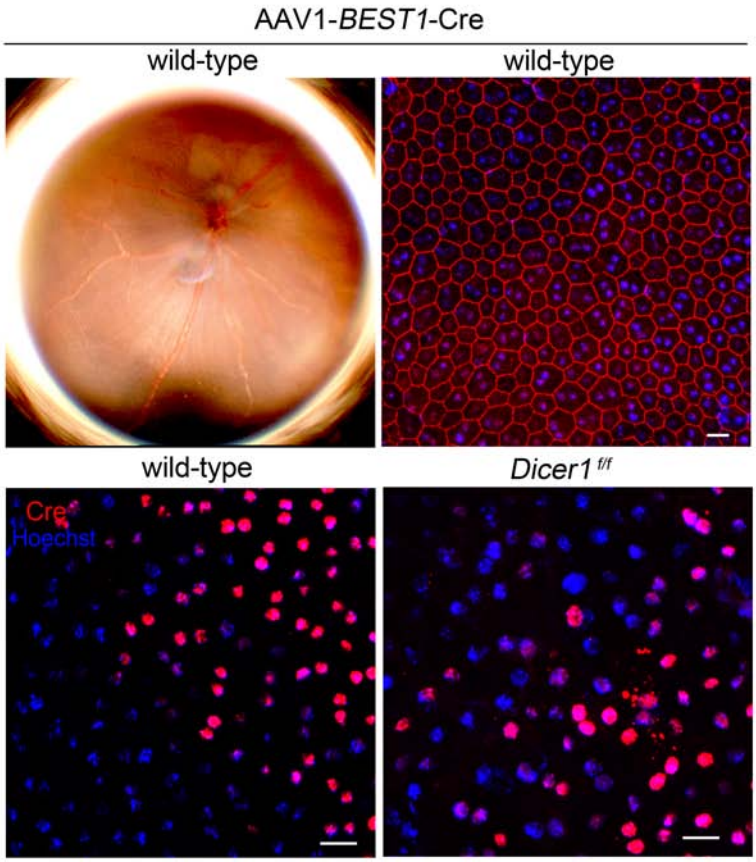


**Cre recombinase expression does not induce retinal pigmented epithelium (RPE) degeneration.** Subretinal administration of adeno-associated viral vector coding for Cre recombinase directed by the BEST1 promoter (AAV1-*BEST1*-Cre) in wild-type mice did not induce retinal toxicity that was evident on fundus photography (top left) and did not disrupt the tiling pattern of the RPE monolayer (top right). Circular flash artefact is seen in the centre of the fundus photograph. RPE cell borders delineated by staining with anti-ZO-1 antibody (red) and nuclei stained by Hoechst 33342 (blue). RPE flat mounts show successful Cre recombinase expression (red) following subretinal injection of AAV1-*BEST1*-Cre in wild-type (bottom left) and *Dicer1*$^{f/f}$ (bottom right) mouse eyes. Representative images shown. n=8–10. Scale bar (20 μm).

**Supplementary Figure 5**

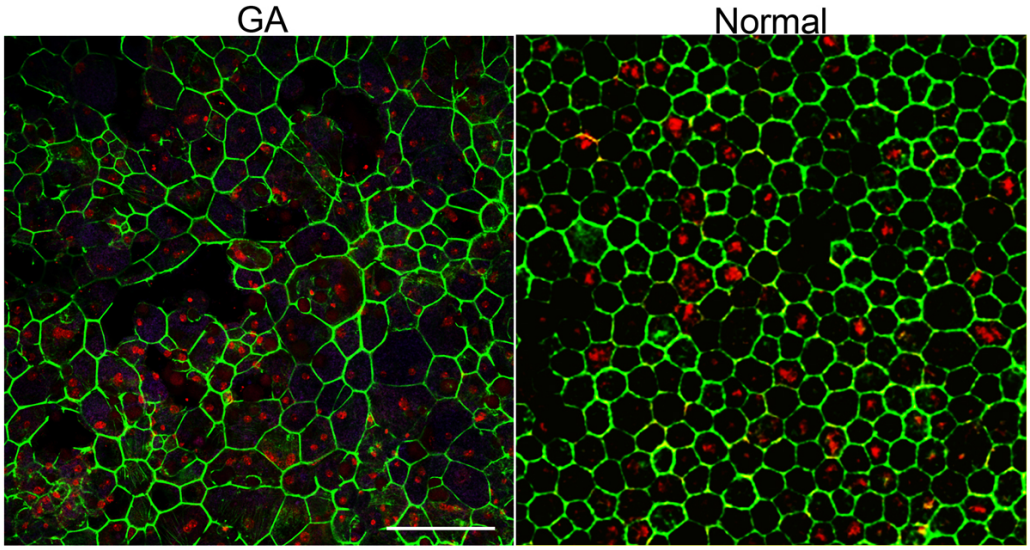


**Retinal pigmented epithelium (RPE) cell dysmorphology in human age-related macular degeneration eye with atrophy.** In contrast to the well tessellated RPE cell monolayer observed in a normal human eye (right), marked changes in RPE cell size and shape are observed in the human eye with geographic atrophy (left). These changes resemble those observed in eyes of mice wherein *Dicer1* has been depleted in the RPE. RPE cell borders delineated by staining with anti-ZO-1 antibody (green) and nuclei stained by propidium iodide (red). Representative image shown. n=8. Scale bar, 50 μm.

**Supplementary Figure 6**

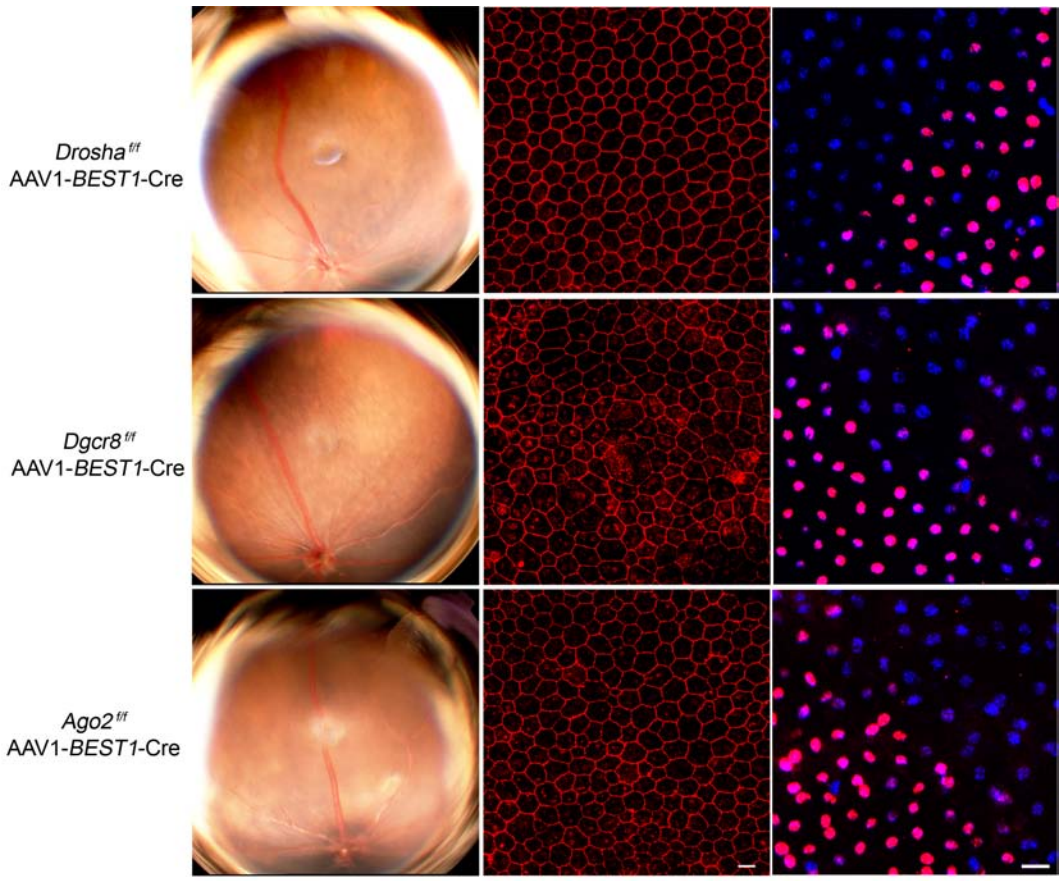


**Conditional ablation of *Drosha*, *Dgcr8*, or *Ago2* in the retinal pigmented epithelium (RPE) does not induce degeneration as seen in *Dicer1*-ablated mice.** Fundus photographs (left column) show no significant degeneration following subretinal injection of AAV-*BEST1*-Cre in mice "floxed" for *Drosha*, *DGCR8*, or *Ago2*. Circular flash artifacts are seen near the centre of the fundus photographs. Injection site wound appears white in the fundus photograph of the *Ago2*$^{f/f}$ eye. RPE flat mounts (middle column) stained with anti-ZO-1 antibody (red) and Hoechst 33342 (blue) show normal tiling pattern of RPE with no gross disturbance of cell size or shape. RPE flat mounts (right column) stained with anti-Cre recombinase antibody (red) and Hoechst 33342 (blue) shows successful Cre expression in these mice eyes. Representative images shown. n=8–12. Scale bar (20 μm).

**Supplementary Figure 7**

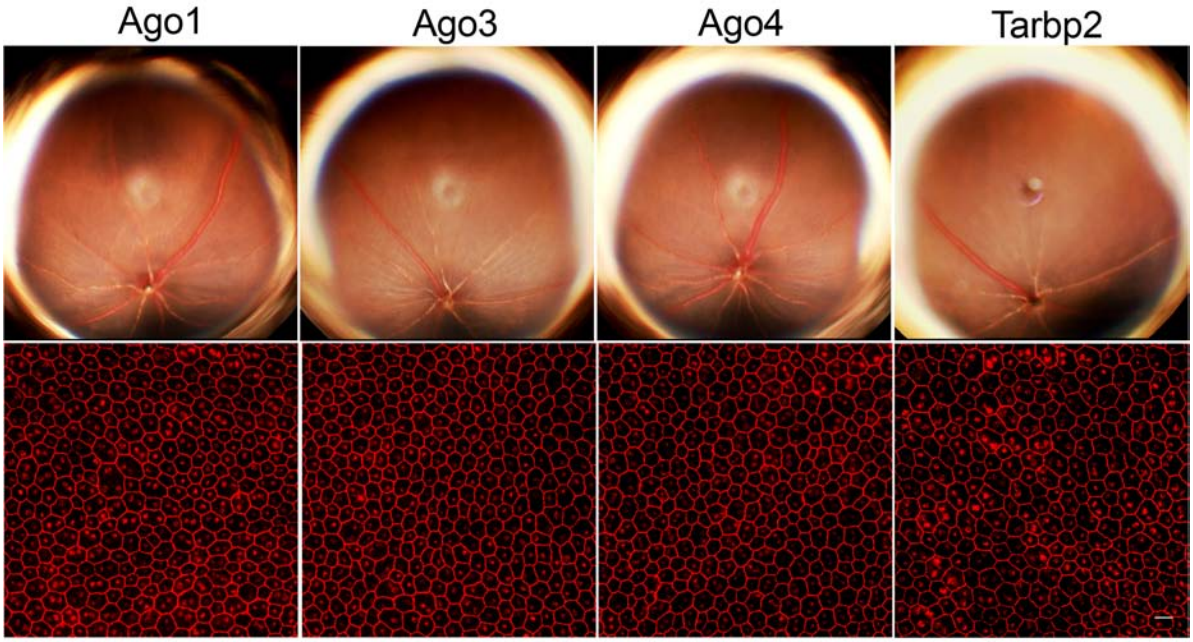


**Deficiency of *Ago1*, *Ago3*, *Ago4*, or *Tarbp2* does not induce RPE degeneration.** Mice deficient in *Ago1 Ago3 Ago4, or Tarbp2* have normal retinal appearance on fundus photography (top row) and normal RPE monolayer architecture on ZO-1 stained (red) flat mounts (bottom row). Circular flash artefact is seen in the centre of the fundus photographs. Scale bar, 20 μm.

**Supplementary Figure 8**

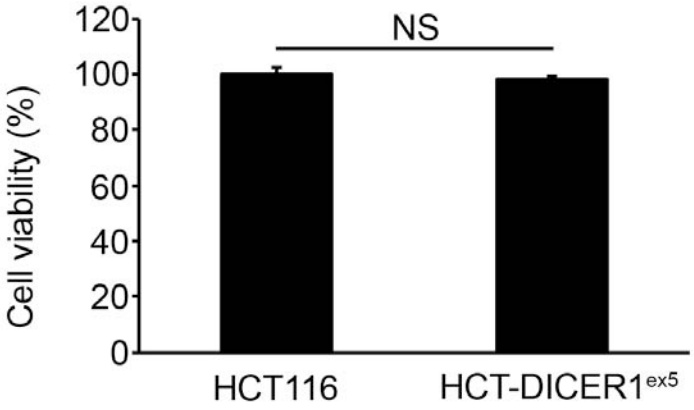


**DICER1 mutant cells impaired in miRNA biogenesis do not have compromised cell viability.** There was no difference in baseline cell viability between HCT-DICER1$^{ex5}$ cells, which are impaired in miRNA biogenesis[1], and parent HCT116 cells over 3 days of analysis of cell proliferation. n=3. NS, not significant.

**Supplementary Figure 9**

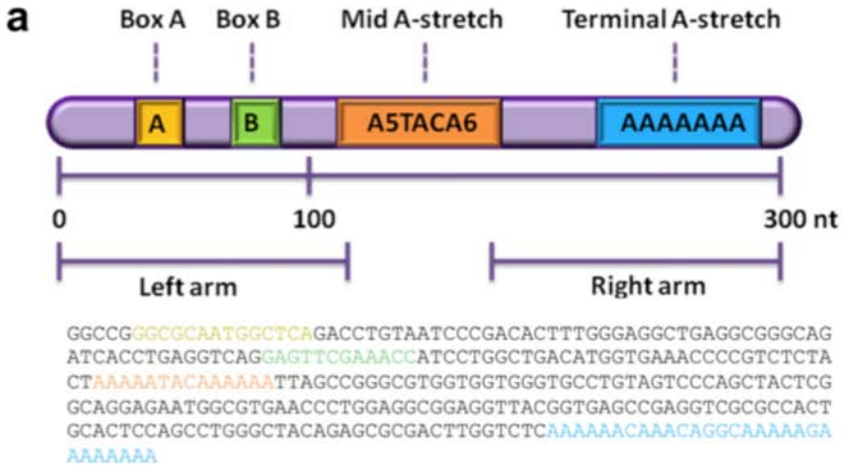


**b**

```
Alu-Sq          GGCCGGGCGCGGTGGCTCACGCCTGTAATCCCAGCACTTTGGGAGGCCGAGGCGGGTGGA 60
Sequence 1      GGCCGGGCGCAATGGCTCAGACCTGTAATCCCGACACTTTGGGAGGCTGAGGCGGGCAGA 60
Sequence 2      ----------------------------ATCCCAGCACTCTGGCAGGCCGAGGCGGGTGGA 33
                                            *****  **** *** **** ********  **

Alu-Sq          TCACCTGAGGTCAGGAGTTCGAGACCAGCCTGGCCAACATGGTGAAACCCCGTCTCTACT 120
Sequence 1      TCACCTGAGGTCAGGAGTTCGAAACCATCCTGGCTGACATGGTGAAACCCCGTCTCTACT 120
Sequence 2      TCA--TGAGGTCAGGAGATCGAGACCATCCCGGCCAACACAGCGAAACCCCATCTCTACT 91
                ***  ************ **** **** ** ***  ***  * ******** ********

Alu-Sq          AAAAA-TACAAAAA-------TTAGCCGGGCGTGGTGGCGGGCGCCTGTAATCCCAGCTA 172
Sequence 1      AAAAA-TACAAAAAA------TTAGCCGGGCGTGGTGGTGGGTGCCTGTAGTCCCAGCTA 173
Sequence 2      AAAAAATACAAAAAGAAAAAATTAGCCAGGTGTGGTGGTGGGCGCCTGTAGTCTCAGCTG 151
                ***** ********       ****** ** ******* *** ******* ** *****

Alu-Sq          CTCGGGAGGCTGAGGCAGGAGAATCGCTTGAACCCGGGAGGCGGAGGTTGCAGTGAGCCG 232
Sequence 1      CTCGG----------CAGGAGAATGGCGTGAACCCTGGAGGCGGAGGTTACGGTGAGCCG 223
Sequence 2      CTCGGGAGGCTGAGGCGGGAGAGTTGCTTGGGCCCGGGAGGCGGAGGTTGCAGTGAGCCG 211
                *****          * ***** * ** **  *** ************* * ********

Alu-Sq          AGATCGCGCCACTGCACTCCAGCCTGGGCAACAAGAGCGAAACTCCGTCTCAAAAAAAA- 291
Sequence 1      AGGTCGCGCCACTGCACTCCAGCCTGGGCTACA-GAGCGCGACTTGGTCTCAAAAAACAA 282
Sequence 2      GGATCACGCC---------------------------------------------------- 221
                 * ** ****

Alu-Sq          --------------------
Sequence 1      ACAGGCAAAAAGAAAAAAAA 302
Sequence 2      --------------------
```

**Human geographic atrophy eye retinal pigmented epithelia contain *Alu* RNA sequences. a,** *Top:* Typical *Alu* element with conserved structural regions (adapted from ref. 2). The left arm consists of RNA polymerase III binding sites (Box A and Box B). The right arm occasionally contains a terminal poly A tail that may be interspersed with non-A bases. The 5' and 3' regions of the Alu element are linked by a mid-stretch A-rich sequence. *Bottom:*

Representative *Alu* cDNA (Sequence 1). The conserved regions mentioned above are highlighted and correspond to the coloured boxes in the *top* figure. **b,** Alignment of *Alu* cDNA Sequences 1 and 2 isolated from human eyes with geographic atrophy to *Alu* Sq consensus sequence. These sequences contain the highly conserved 5' *Alu* consensus elements (5' characteristic *Alu* region – blue; RNA polymerase III promoter B box – red), with extensive heterogeneity located 3' to the mid-sequence poly-A stretch that have been reported to exist in *Alu* sequences[3,4].

**Supplementary Figure 10**

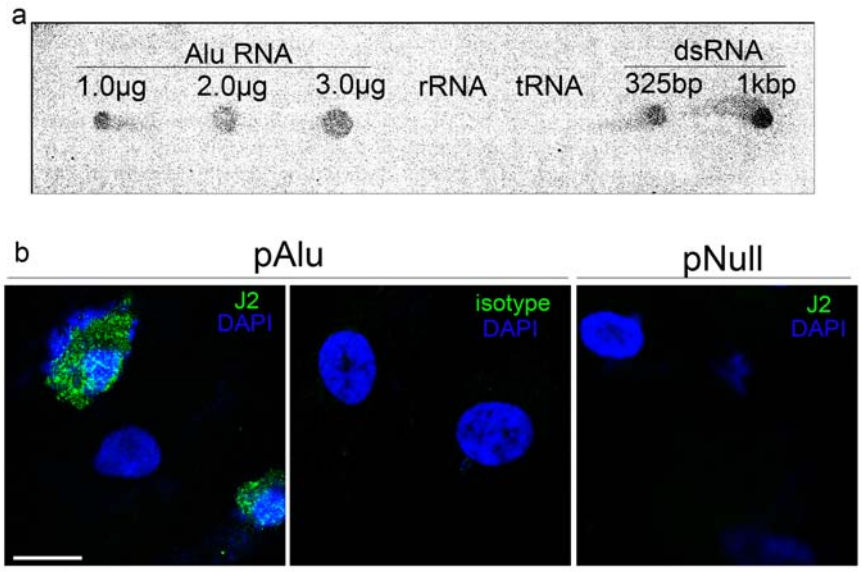


**J2 anti-dsRNA antibody recognizes *Alu* RNA. a,** *Alu* RNA duplex isolated and cloned from the retinal pigmented epithelium (RPE) of a human eye with geographic atrophy was recognized by J2 anti-dsRNA antibody in an immuno-dot blot format. J2 antibody did not recognize rRNA or tRNA (negative controls), but did recognize RNA duplexes of 325-bp or 1-kbp in length (positive controls). **b,** Immunofluorescent imaging of human RPE cells transfected with pAlu shows that J2 recognizes *Alu* expressed in these cells (left panel). Specificity of staining confirmed by absence of staining with isotype control antibody (middle panel) and by the absence of immunodetection following transfection with pNull (right panel). Representative images shown. n=3. Scale bar (20 µm).

**Supplementary Figure 11**

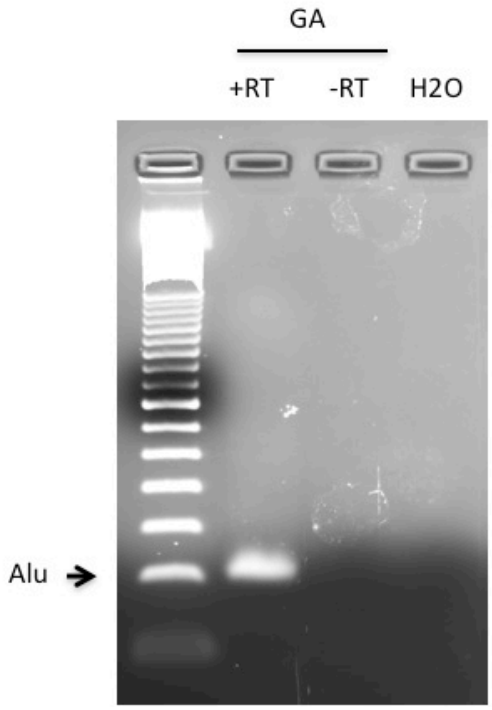


**Confirmation of lack of DNA contamination in *Alu* RNA PCR.** The relative abundance of *Alu* RNA in the RPE of human eyes with human geographic eyes was presented in Fig. 2f. Shown above is the detection of the PCR product band for a sample of human geographic atrophy RPE that underwent reverse transcription (RT+). No amplification was detected in the negative controls where reverse transcriptase (RT–) was omitted or where water alone was analyzed. These data demonstrate the absence of DNA contamination in the sample.

**Supplementary Figure 12**

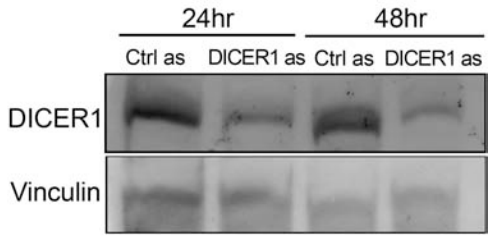


**Validation of DICER1 knockdown.** Transfection of DICER1 antisense oligonucleotides (as) into human RPE cells knocks down DICER1 protein abundance, as monitored by Western blot analysis, over 2 days. Efficiency of protein loading is monitored by blotting for the housekeeping Vinculin protein. Representative of 3 experiments.

**Supplementary Figure 13**

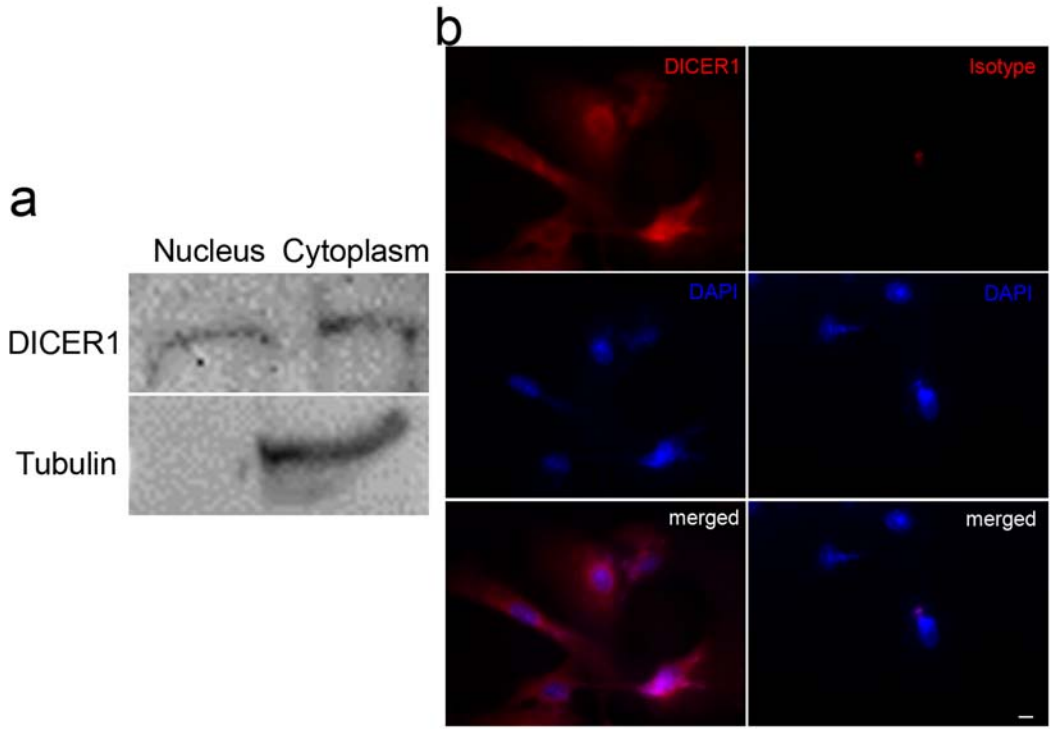


**DICER1 is expressed in nucleus and cytoplasm. a,** Western blot shows expression of DICER1 in both the nuclear and cytoplasmic fractions of human RPE cells. Blotting of the same protein sample reveals the presence of Tubulin in the cytoplasmic fraction and not in the nuclear fraction. **b,** Merged images (bottom row) of DICER1 immunofluorescence (red, top row) and nuclear DAPI fluorescence (middle row) confirm expression of DICER1 in both the nucleus and the cytoplasm of human RPE cells. Representative images shown. Scale bar, 10 μm.

**Supplementary Figure 14**

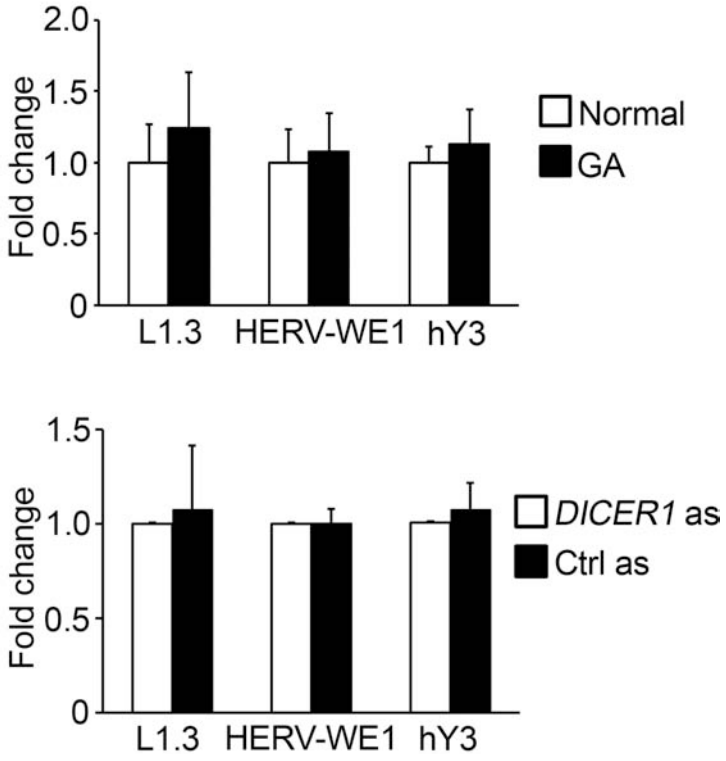


**Retrotransposons and repetitive RNAs are not generically activated in geographic atrophy or by DICER1 depletion.** In the RPE of human eyes with geographic atrophy (GA, n=7), there was no significant increase in the abundance of RNAs coded by LINE L1.3, a long interspersed repetitive element, human endogenous retrovirus-W envelope (HERV-WE1), a long terminal repeat retrotransposon, or hY3, a repetitive small cytoplasmic Ro RNA compared to normal human eyes (top, n=8). These RNAs also were not upregulated by *DICER1* antisense (as) knockdown, compared to control (Ctrl) as treatment, in human RPE cells (bottom). n=3. Transcript abundance monitored by real-time RT-PCR and normalized to 18S rRNA levels.

**Supplementary Figure 15**

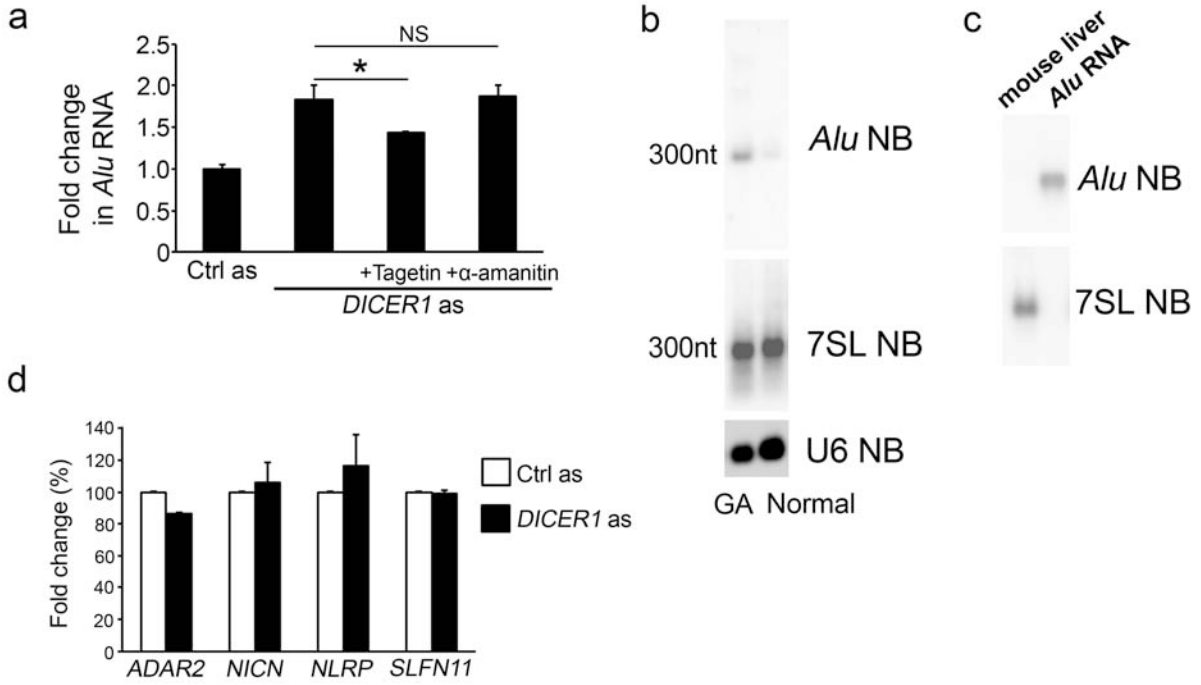


***Alu* RNA induced by *DICER1* depletion is RNA Pol III derived. a,** The upregulation of *Alu* RNA in RPE cells treated with antisense (as) oligonucleotides targeting *DICER1*, compared to control (Ctrl), is inhibited by treatment with the Pol III inhibitor tagetitoxin (tagetin), but not by the Pol II inhibitor α–amanitin. *, $P<0.05$, NS, not significant, compared to treatment with *DICER1* as treatment alone. **b,** Northern blot (NB) shows that the abundance of *Alu* RNA species in the RPE of a human eye with geographic atrophy (GA) is greater than in normal human eye RPE, and is principally approximately 300 nucleotides long, consistent with the length of a non-embedded Pol III derived transcript. Reprobing these samples with a probe corresponding to the "S region" of the 7SL RNA gene that is not present in *Alu* elements shows that 7SL RNA abundance is not different between the RPE of normal and GA human eyes. Abundance of U6 RNA in GA and normal eyes shows loading efficiency. **c,** Northern blot shows that *Alu* probe detects *in vitro* transcribed *Alu* RNA but not 7SL RNA in mouse liver (which lacks primate-specific *Alu*), and reprobing these samples

confirms specificity of the 7SL probe. **d,** *DICER1* knockdown by antisense (as) oligonucleotides in human RPE cells does not, compared to control (Ctrl) as treatment, induce upregulation of several Pol II-transcribed genes (*ADAR2*, *NICN*, *NLRP*, *SLFN11*) that contain embedded *Alu* sequences in their exons. n=3.

**Supplementary Figure 16**

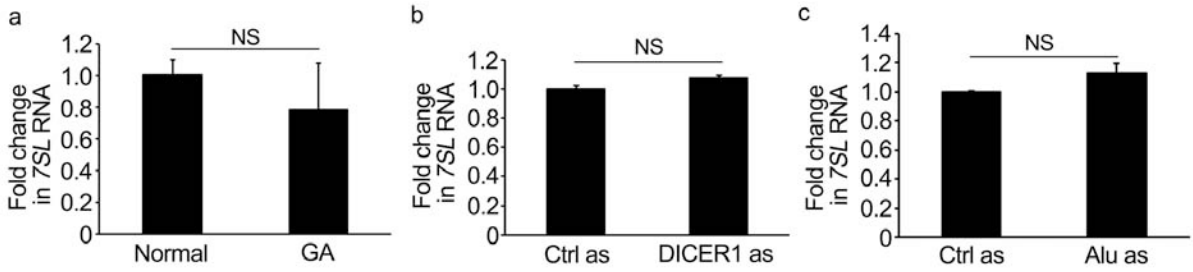


**7SL RNA is not regulated in geographic atrophy or by inhibition of DICER1 or *Alu*. a,** 7SL RNA abundance was not different in the RPE of human eyes with geographic atrophy (GA) compared to the RPE of normal human eyes without GA (n=8). **b,** 7SL RNA abundance was not different in human RPE cells transfected with antisense oligonucleotide (as) targeting DICER1 from those transfected with control (Ctrl) as. n=3. **c,** 7SL RNA abundance was not different in human RPE cells transfected with antisense oligonucleotide (as) targeting *Alu* from those transfected with control (Ctrl) as. n=3. 7SL RNA abundance, relative to 18S rRNA, was monitored by real-time RT-PCR. NS, not significant by Student t test.

**Supplementary Figure 17**

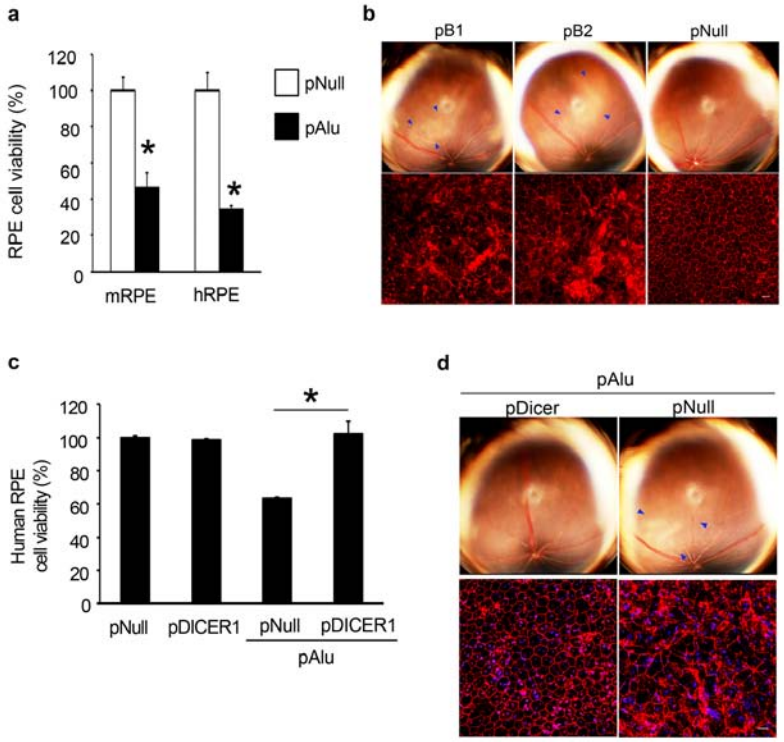


***Alu*/B1/B2 RNA-induced RPE degeneration blocked by DICER1 overexpression. a,** Plasmid coding for *Alu* RNA (pAlu) reduced mouse and human RPE cell viability (mRPE or hRPE). **b,** Subretinal transfection of pB1 or pB2 RNAs, but not of pNull, induces RPE degeneration in wild-type mice. Top row shows fundus photographs demonstrating areas of degeneration outlined by blue arrowheads. Bottom row shows ZO-1 stained (red) RPE flat mounts demonstrated marked degeneration and disarray of the RPE cells in mice overexpressing B1 or B2 RNAs. Circular flash artefact is seen in the centre of the fundus photographs. n=4. Representative images shown. Scale bar, 20 μm. **c,** hRPE cytotoxicity induced by pAlu inhibited by pDICER1 but not pNull. **d,** Subretinal pDICER1, but not pNull, inhibited pAlu induced wild-type mouse RPE degeneration. **(a,c**) Values normalized to pNull or vehicle. * $P < 0.05$ by Student t test. (**a**–**c**) n=4–6. (**d**) n=10.

**Supplementary Figure 18**

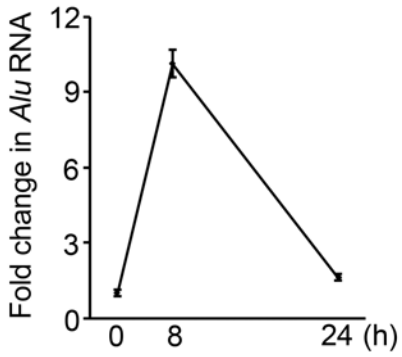


***Alu* RNA enters retinal pigmented epithelium (RPE) cells *in vivo*.** Subretinal administration of *Alu* RNA in wild-type mice achieved RPE cell delivery at 8 h after injection as monitored by real-time RT-PCR in isolated cell lysates (n=3).

**Supplementary Figure 19**

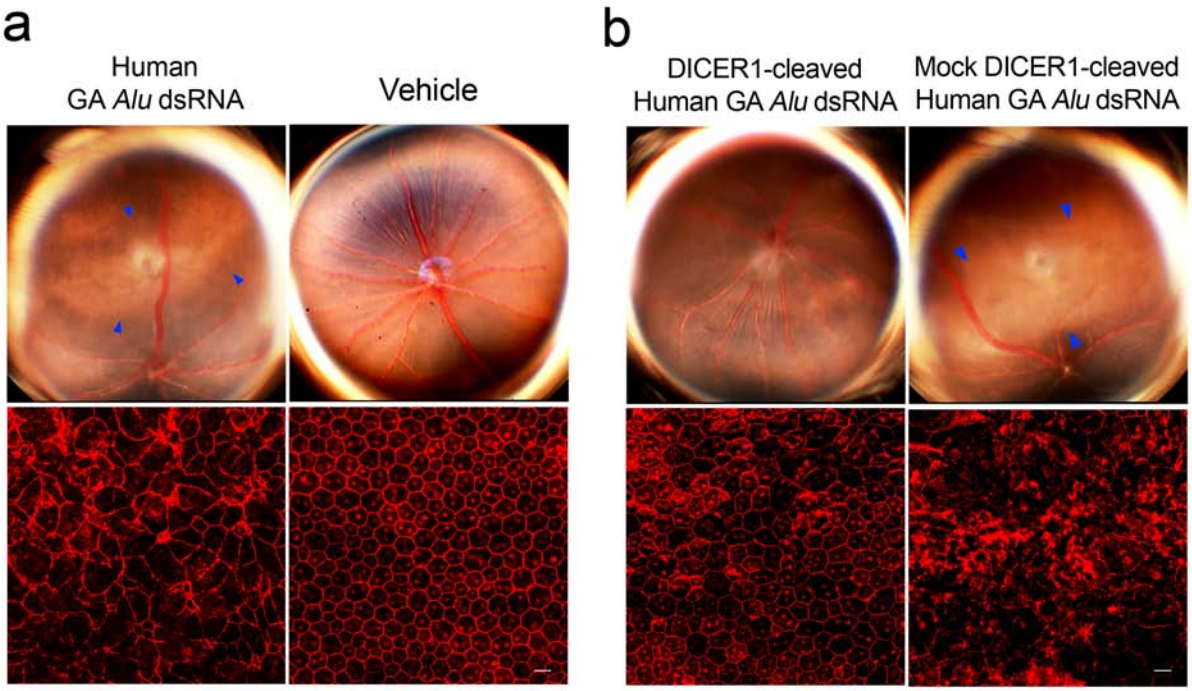


**Human GA *Alu* dsRNA does not induce RPE degeneration when cleaved by DICER1. a,** Subretinal administration of a fully complementary synthetic *Alu* RNA (dsRNA) corresponding to the sequence of an *Alu* RNA isolated from a human eye with geographic atrophy (GA) induces RPE degeneration in wild-type mice. Vehicle administration does not damage the retina. Top panels show fundus photographs with the area of RPE degeneration outlined by blue arrowheads. Circular flash artefact is seen in the centre of the fundus photographs. Bottom panels show ZO-1 stained (red) RPE flat mounts that are well arrayed in vehicle (bottom) but disorganized in *Alu* dsRNA (top). **b,** This *Alu* dsRNA did not induce RPE degeneration when it was first subjected to cleavage by recombinant DICER1. However, when subjected to mock cleavage by DICER1, this *Alu* dsRNA did induce RPE degeneration. n=4. Representative images shown. Scale bar, 20 μm.

**Supplementary Figure 20**

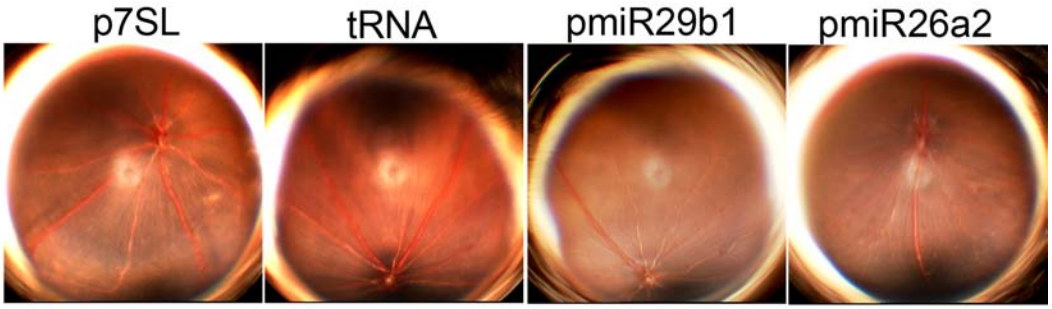


**RPE degeneration does not occur in response to a variety of structured RNAs.**

Subretinal transfection of transfer RNA (tRNA) or of plasmids coding for 7SL RNA, pri-miRNA-29b1 or pri-miRNA26a2 in wild-type mice did not induce retinal toxicity that was evident on fundus photography. Circular flash artefact is seen in the centre of the fundus photographs. N=4. Representative images shown.

**Supplementary Figure 21**

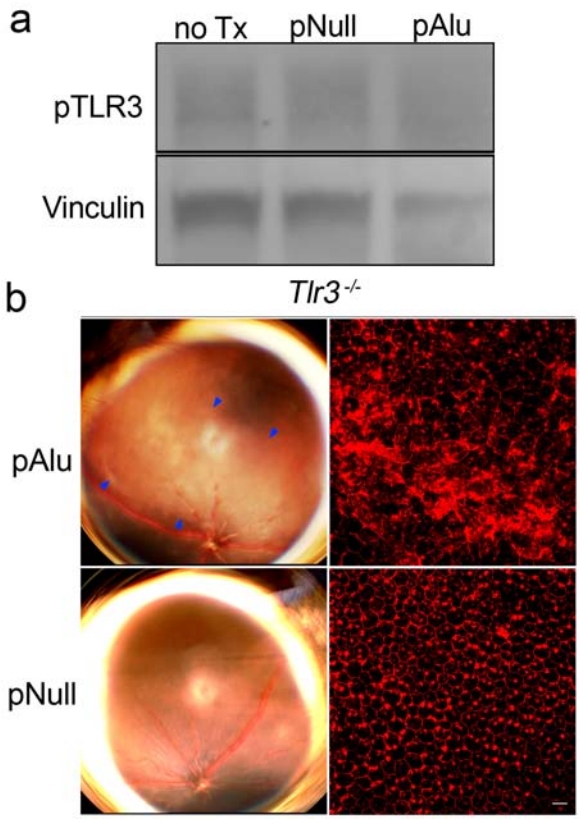


***Alu* RNA does not cause RPE degeneration via TLR3. a,** Western blot shows that transfection of pAlu or pNull does not induce TLR3 phosphorylation, relative to the levels of the housekeeping protein Vinculin, in human RPE cells. **b,** Subretinal transfection of pAlu induced RPE degeneration in *Tlr3*-/- mice where pNull transfection did not do so. Representative images shown. n=4. Scale bar, 20 μm.

**Supplementary Figure 22**

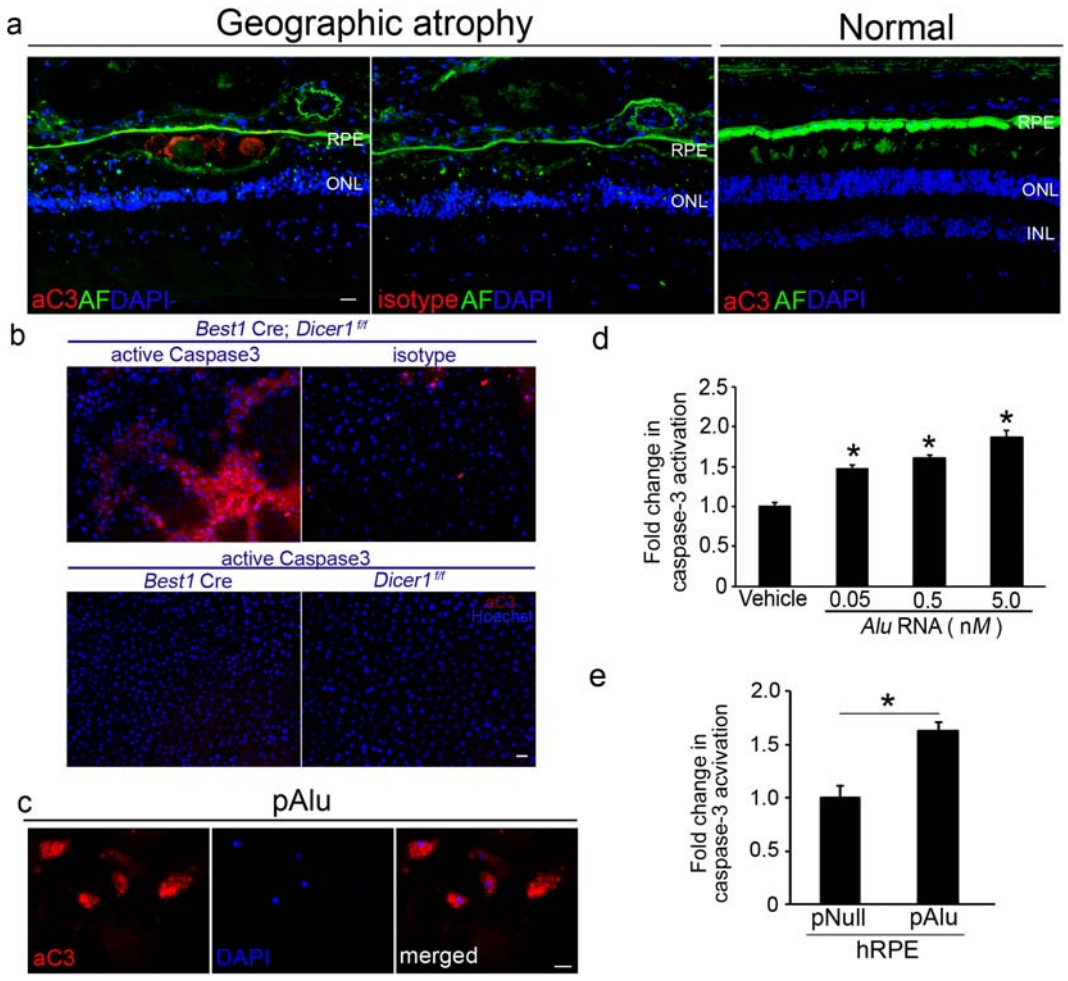


**DICER1 reduction or *Alu* RNA augmentation induces caspase-3 activation. a,** Immunolocalization of activated caspase-3 (red) in the RPE of human eyes with geographic atrophy (left panel). Specificity of immunolabeling revealed by absence of staining with isotype control antibody (middle panel) and in control eyes stained with antibody against cleaved caspase-3 (right panel). Autofluorescence of RPE and choroid seen in green channel. Nuclei stained by DAPI (blue). **b,** Flat mounts of *BEST1* Cre; *Dicer1*$^{f/f}$ mice show evidence of caspase-3 activation (red staining, top left panel). Specificity of immunolabeling revealed by absence of staining with isotype control antibody (top right panel). No caspase-3 activation was detectable in the RPE of littermate control *BEST1* Cre or *Dicer1*$^{f/f}$ mice

(bottom panels). **c,** Human RPE cells transfected with pAlu showed evidence of caspase-3 activation (red staining, top left panel). DAPI (blue staining) and merged images are also shown. Scale bars (20 μm, **a,b**; 10 μm, **c**). Representative images shown. n=4–6. **d,** Exposure of human RPE cells to *Alu* RNA induced dose-dependent increase in caspase-3 activation, as monitored by fluorometric plate assay. n=3, * $P < 0.05$ compared to vehicle by Student t test. **e,** Transfection of human RPE cells with pAlu induced increase in caspase-3 activation. n=3, * $P = 0.47$ by Student t test.

**Supplementary Figure 23**

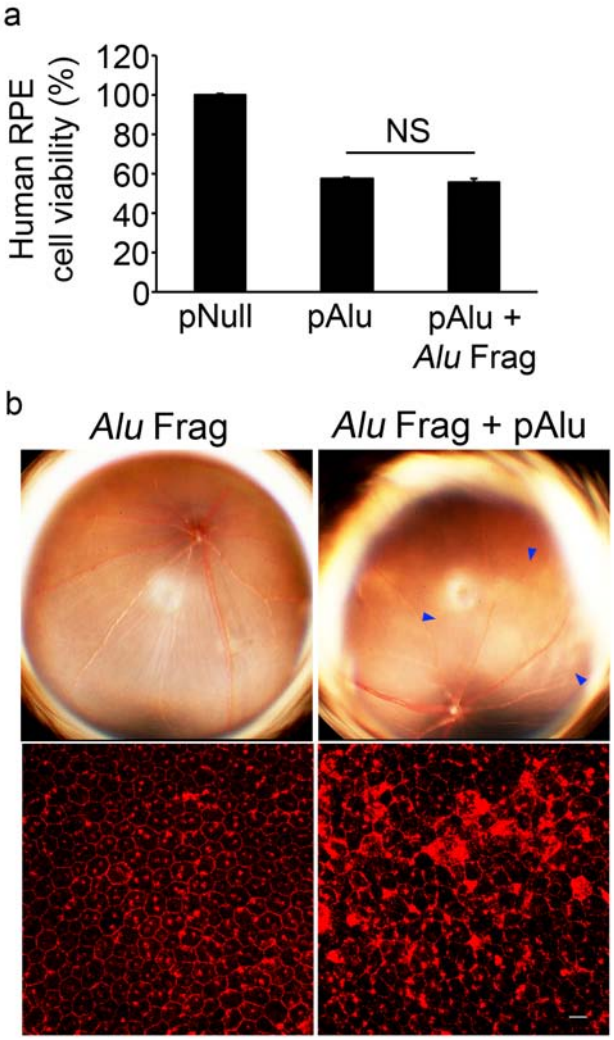


***Alu* RNA cleavage fragments do not modulate RPE degeneration. a,** Transfection of pAlu induced cell death in human RPE cells. Cotransfection of DICER1-cleaved *Alu* RNA fragments did not change the degree of cell death. n=3. **b,** Subretinal transfection of DICER1-cleaved *Alu* RNA fragments (Frag) in wild-type mice did not cause RPE degeneration as seen by fundus photography (top left) or ZO-1-stained (red) RPE flat mounts (bottom left). Cotransfections of these fragments did not prevent the RPE degeneration induced by pAlu in wild-type mice (right panels). n=4. Representative images shown. Scale bar, 20 μm.

**Supplementary Figure 24**

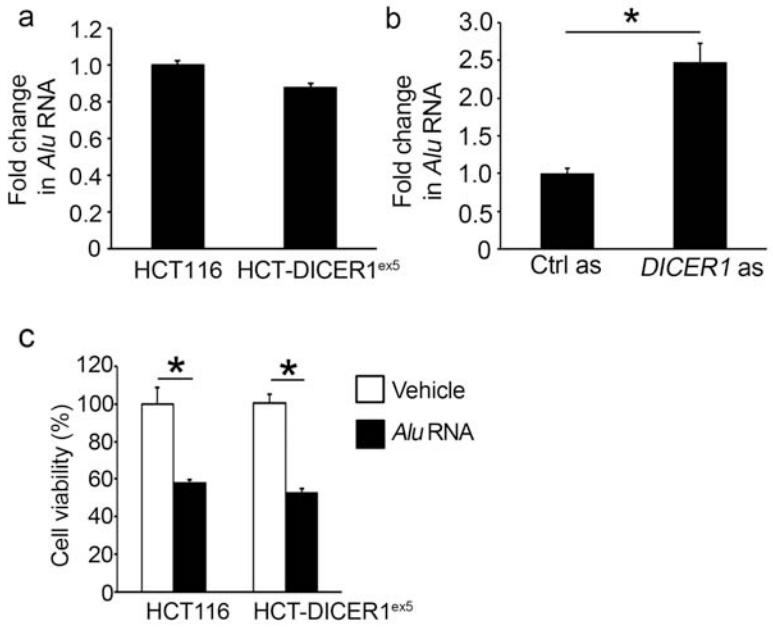


**Impaired DICER1 processing of microRNAs does not increase *Alu* RNA abundance or modulate *Alu* RNA cytotoxicity. a,** There was no significant difference ($P$>0.05) in *Alu* RNA transcript abundance between HCT116 parent cells and HCT mutant cells carrying a mutation in exon 5 (ex5) of DICER1 which renders it incapable of processing microRNAs. **b,** Transfection of anti-sense oligonucleotide (as) targeting DICER1 into HCT116 cells increased the abundance of *Alu* RNA transcripts compared to control anti-sense oligonucleotide (Ctrl as) at 48 h. Transcript abundance monitored by real-time RT-PCR and normalized to 18S rRNA levels. **c,** *Alu* RNA induced similar levels of cell death in HCT116 parent and HCT-DICER1$^{ex5}$ cells. * $P$<0.05 by Student t test. n=4–6.

**Supplementary Figure 25**

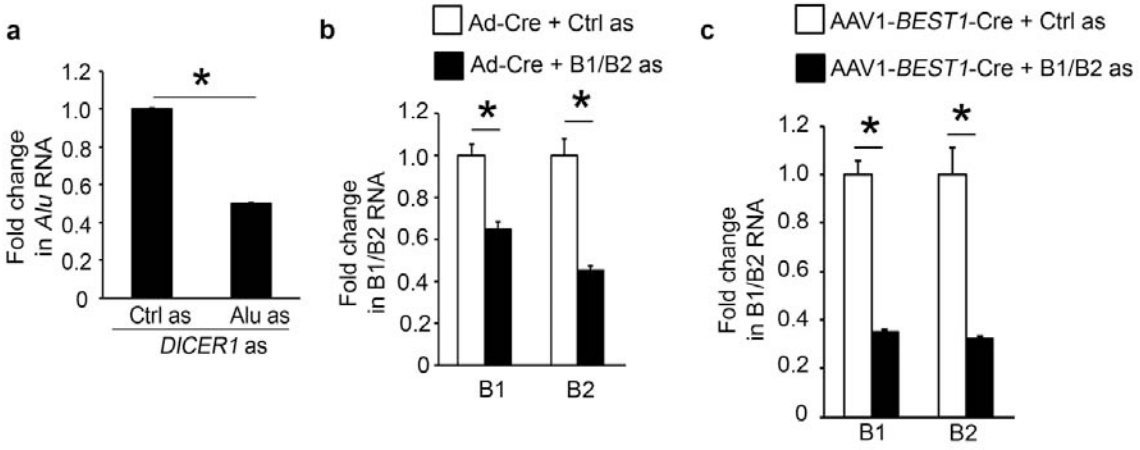


**a,** *Alu* RNA antisense (as), compared to control (Ctrl) as, inhibited *Alu* RNA accumulation in human RPE cells induced by DICER1 as. **b,** B1/B2 RNA as, compared to control (Ctrl) as, inhibited B1/B2 RNA accumulation in *Dicer1*$^{f/f}$ mouse RPE cells infected by adenoviral vector coding for Cre recombinase (Ad-Cre). **c,** Subretinal AAV-*BEST1*-Cre induced accumulation of B1/B2 RNAs in the RPE of *Dicer1*$^{f/f}$ mice was inhibited by subretinal cholesterol-conjugated B1/B2 as compared to cholesterol-conjugated Ctrl as. * $P < 0.05$ by Student t test. n=4–6 (**a,b**). n=8 (**c**).

**Supplementary Figure 26**

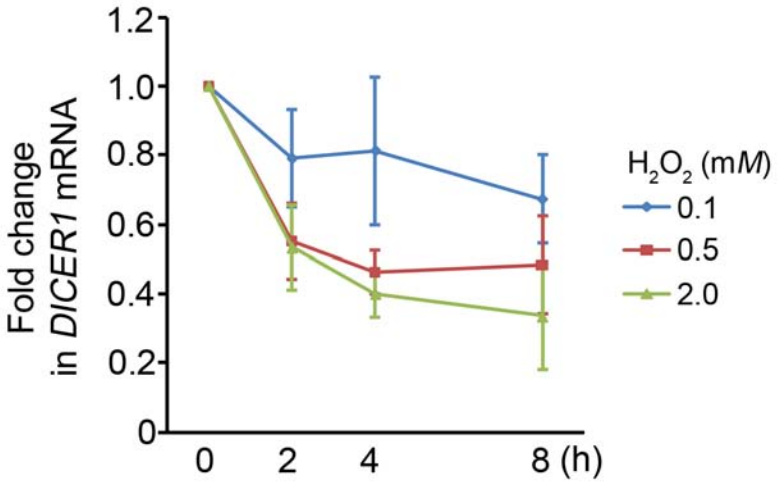


**Oxidative stress downregulates *DICER1* in human RPE cells.** Human retinal pigmented epithelium (RPE) cells exposed to varying concentrations of hydrogen peroxide ($H_2O_2$) display a dose- and time-dependent reduction in *DICER1* mRNA abundance, as monitored by real-time RT-PCR and normalized to 18S rRNA levels. n=3.

## Supplemental Notes

*Dicer1* mRNA levels are not modulated in multiple mouse models of retinal degeneration including light damage[5,6], hyperoxia[7], retinal detachment[5,8], *Crx*$^{-/-}$ mice[9], *Rs1h*$^{-/-}$ mice[10], *rd1* mice[11,12], *cpfl1* mice[13], or *Mitf* mice[14]. *Dicer1* abundance also is not reduced in mouse models of cellular stress in the retina including exposure to advanced glycation endproducts[15] or retinal detachment[16]. Therefore, *Dicer1* downregulation is not a generic late-stage stress response in the retina.

## Materials and methods

### Animals

All animal experiments were approved by institutional review committees and the Association for Research in Vision and Ophthalmology. C57Bl/6J and *Dicer1*$^{f/f}$ mice were purchased from The Jackson Laboratory. Transgenic mice that express Cre recombinase in the retinal pigmented epithelium under the control of the human bestrophin-1 promoter (*BEST1* Cre mice), *DGCR8*$^{f/f}$, *Drosha*$^{f/f}$, *Tarbp2*$^{-/-}$, *Ccl2*$^{-/-}$ *Ccr2*$^{-/-}$, and *Cp*$^{-/-}$ *Heph*$^{-/-}$ mice have been previously described[17-23]. *Ago2*$^{f/f}$ mice[24] and mice deficient in *Ago1*, *Ago3*, or *Ago4* (ref. 25) were generously provided by A. Tarakhovsky. For all procedures, anaesthesia was achieved by intraperitoneal injection of 50 mg/kg ketamine hydrochloride (Ft. Dodge Animal Health) and 10 mg/kg xylazine (Phoenix Scientific), and pupils were dilated with topical 1% tropicamide (Alcon Laboratories).

**Fundus photography.** Retinal photographs of dilated mouse eyes were taken with a TRC-50 IX camera (Topcon) linked to a digital imaging system (Sony).

**Human tissue.** Donor eyes or ocular tissues from patients with geographic atrophy due to AMD or patients without AMD were obtained from various eye banks in Australia and the United States of America. These diagnoses were confirmed by dilated ophthalmic examination prior to acquisition of the tissues or eyes or upon examination of the eye globes post mortem. The study followed the guidelines of the Declaration of Helsinki. Institutional review boards granted approval for allocation and histological analysis of specimens.

**Immunolabeling.** Human eyes fixed in 2–4% paraformaldehyde were prepared as eyecups, cryoprotected in 30% sucrose, embedded in optimal cutting temperature compound (Tissue-Tek OCT; Sakura Finetek), and cryosectioned into 10 μm sections. Depigmentation was achieved using 0.25% potassium permanganate and 0.5% oxalic acid. Immunohistochemical staining was performed with the mouse antibody against dsRNA (1:1,000, clone J2, English & Scientific Consulting) or rabbit antibody against human DICER1 (1:100, Santa Cruz Biotechnology). Isotype IgG was substituted for the primary antibody to assess the specificity of the staining. Bound antibody was detected with biotin-conjugated secondary antibodies (Vector Laboratories). Slides were further incubated in alkaline phosphatase-streptavidin solution (Invitrogen) and the enzyme complex was visualized by Vector Blue (Vector Laboratories). Levamisole (Vector Laboratories) was used to block endogenous alkaline phosphatase activity. Slides were washed in PBS, rinsed with deionized water, air-dried, and then mounted in Clear Mount (EMS). Mouse RPE/choroid flat mounts were fixed with 4% paraformaldehyde or 100% methanol and stained with rabbit antibodies against human zonula occludens-1 (1:100, Invitrogen), Cre recombinase (1:1000, EMD4Biosciences), or human cleaved caspase-3 (1:200, Cell Signaling) and visualized with Alexa594- or Cy5-conjugated secondary antibodies. Both antibodies are cross-reactive

against the mouse homologues. Primary human RPE cells were grown to 70-80% confluency in chamber slides (Lab-Tek). After 24 h of transfection with pAlu or pUC19, cells were fixed in acetone for 10 min at –20 °C. Cells were blocked with PBS-3%BSA and incubated with mouse antibody against dsRNA (1:500, clone J2) overnight at 4 °C and visualized with Alexa Fluor 488-conjugated secondary antibodies. For DICER1 staining, cells were fixed in methanol/acetone (7:3) for 30 min on ice, blocked with PBS-3%BSA-5%FBS, incubated with rabbit antibody against human DICER1 (1:100, Santa Cruz Biotechnology) overnight at 4 °C, and visualized with goat-anti-rabbit Alexa Fluor 594-conjugated secondary antibodies. After DAPI counterstaining, slides were cover slipped in Vectashield (Vector Laboratories). Images were obtained using the Leica SP-5 or Zeiss Axio Observer Z1 microscopes.

**Histology.** Mouse eyes were fixed with 4% paraformaldehyde and 3.5% glutaraldehyde, postfixed in 2% osmium tetroxide, and dehydrated in ethanol and embedded. Semi-thin (1 μm) sections were cut and stained with toluidine blue. Bright field images were obtained using the Zeiss Axio Observer Z1 microscope.

**Subretinal injection.** Subretinal injections (1 μL) in mice were performed using a Pico-Injector (PLI-100, Harvard Apparatus). *In vivo* transfection of plasmids coding for *DICER1* (ref. 26), *Alu* Ya5 (ref. 27), *Alu* Yb9 (ref. 28), 7SL RNA (ref. 29), pri-miR29b1 (Addgene), or pri-miR26a2 (Addgene) and bovine tRNA (Sigma-Aldrich) (0.5 mg/mL) was achieved using 10% Neuroporter (Genlantis). AAV1-*BEST1*-Cre[30] or AAV1-*BEST1*-GFP were injected at $1.0\times10^{11}$ pfu/mL and recombinant *Alu* RNAs (1: a single RNA strand of 281 nucleotides whose sequence is that of the cDNA clone TS 103 (ref. 3) and folds into a defined secondary structure identical to a Pol III derived transcript; 2: a single RNA strand of 302 nucleotides whose sequence is identical to that of a clone isolated from the RPE of a

human eye with geographic atrophy that folds into a defined secondary structure identical to a Pol III derived transcript; or 3: a fully complementary dsRNA version of this 302 nucleotide long sequence that mimics a Pol II derived transcript) was injected at 0.3 mg/mL. Cell-permeating cholesterol conjugated-B1/B2 antisense oligonucleotides (as) (5'-TCAGATCTCGTTACGGATGGTTGTGA-3') or cholesterol conjugated-control as (5'-TTGGTACGCATACGTGTTGACTGTGA-3') (both from Integrated DNA Technologies) were injected (2 μg in 1 μL) 10 days after AAV1-BEST1-Cre was injected in *Dicer1*$^{f/f}$ mice.

**Isolation of dsRNA.** Human eyes were stored in RNAlater (Ambion). Tissue extracts were prepared by lysis in buffer containing 50 mM Tris-HCl, pH 8, 150 mM NaCl, 1% Nonidet P-40, protease and phosphatase inhibitors (complete mini EDTA-free, protease inhibitor and phosphatase inhibitor cocktail tablets, Roche), and RNase inhibitor (SUPERase-In, Ambion). After homogenization using bullet blender (Nextadvance) and centrifugation, immunoprecipitations were performed by adding 40 μg of mouse antibody against dsRNA (clone J2) for 16 h at 4 °C. Immunocomplexes were collected on protein A/G agarose (Thermoscientific) and dsRNA species were separated and isolated using Trizol (Invitrogen) according to the manufacturer's instructions.

**Ligation of dsRNA and anchor primer.** An anchor primer (PC3-T7 loop, 5'-p-GGATCCCGGGAATTCGGTAATACGACTCACTATATTTTTATAGTGAGTCGTATTA-OH-3', 200-400 ng, IDT)[31,32] was ligated to dsRNA (200-400 ng) in 50 mM HEPES/NaOH, pH 8 (vWR), 18 mM $MgCl_2$ (Invitrogen), 0.01% BSA (Fisher Scientific), 1 mM ATP (Roche), 3 mM DTT (Fluka), 10% DMSO (Finnzymes), 20% PEG 6000 (Alfa Aesar), and 30U T4 RNA ligase (Ambion). Ligation was performed at 37 °C for 16 h, and ligated dsRNA was purified by MinElute Gel extraction columns (Qiagen).

**Sequence-independent cDNA synthesis.** After denaturation, ligated dsRNA was reverse transcribed in a RT reaction containing 50 mM Tris-HCl, pH 8.3, 10 mM $MgCl_2$, 70 mM KCl, 30 mM β-mercaptoethanol, 1 mM dNTPs and 15U cloned AMV reverse transcriptase (Invitrogen). The mixture was incubated in a thermal cycler (Eppendorf) at 42 °C for 45 min followed by 55 °C for 15 min.

**Polymerase chain reaction (PCR) amplification.** Amplification of cDNA was performed using primer PC2 (5'-p-CCGAATTCCCGGGATCC-3', IDT) in a reaction buffer containing 5 µL cDNA and 40 µL Platinum PCR SuperMix (Invitrogen). The PCR cycling parameters consisted of one step of 72 °C for 1 min to fill incomplete cDNA ends and produce intact DNA, followed by one step of initial denaturation (94 °C, 2 min), 39 cycles of 94 °C for 30 s, 53 °C for 30 s, and 72 °C for 1 min, and a final extension step of 72 °C for 10 min. *In vitro* transcribed dsRNAs of varying lengths (325 bp, 1 and 2 kb) were used as positive controls.

**Cloning and sequencing.** The amplified cDNA products were incubated with 1U calf intestinal alkaline phosphatase (Invitrogen) at 37 °C for 5 min to remove the 5'-phosphate group, separated on a low-melting point agarose gel (1%) and purified using Qiaquick gel extraction kit (Qiagen). The purified dephosphorylated cDNA fragments were cloned in PCRII TOPO vector (Invitrogen) and sequenced using M13 forward (-20) and M13 reverse primers at the University of Kentucky Advanced Genetic Technologies Center using multi-colour fluorescence based DNA sequencer (ABI 3730xl). Sequences were assembled using ContigExpress from vector NTI Advance. The homology of our isolated cDNA sequences to known Alu consensus sequences was determined using the CENSOR server[33] (a WU-BLAST-powered database of repetitive elements ( http://www.girinst.org/censor). For each cDNA sequence, the homologous region of the query was aligned to the consensus *Alu*

sequence using BLASTn[34] (http://www.ncbi.nlm.nih.gov/BLAST). Multiple sequence alignment was performed using ClustalW2 (http://www.ebi.ac.uk/Tools/clustalw2). The consensus sequences have been deposited in GenBank under the accession numbers HN176584 and HN176585.

***Alu* RNA Synthesis.** We synthesized two *Alu* RNAs: a 281 nt *Alu* sequence originating from the cDNA clone TS 103 which is known to be expressed in human cells[3] and a 302 nt *Alu* sequence isolated from the RPE of a human eye with geographic atrophy. Both of these *Alu* RNAs were synthesized using a RNA polymerase T7 promoter and runoff transcription followed by gel purification as previously described[35]. This yields single stranded RNAs that fold into a defined secondary structure identical to Pol III derived transcripts. We also synthesized a fully complementary dsRNA form (resembling a Pol II derived transcript) of the 302 nt human geographic atrophy *Alu* using linearized PCRII TOPO plasmid templates using T7 or SP6 RNA polymerases (MegaScript, Ambion) according to the manufacturer's recommendations. After purification, equal molar amount of each transcript were combined and heated at 95 °C for 1 min, cooled and then annealed at room temperature for 24 h. The *Alu* dsRNA was precipitated, suspended in water and analyzed on 1.4% non-denaturing agarose gel using the single-stranded complementary strands as controls.

**Real-time PCR.** Total RNA was extracted from tissues or cells using Trizol reagent (Invitrogen) according to manufacturer's recommendations and were treated with RNase free DNase (Ambion). Total RNA (1 μg) was reverse transcribed as previously described[22] using qScript cDNA SuperMix (Quanta Biosciences). The RT products (cDNA) were amplified by real-time quantitative PCR (Applied Biosystems 7900 HT Fast Real-Time PCR system) with Power SYBR green Master Mix. Oligonucleotide primers specific for *DICER1* (forward 5'-

CCCGGCTGAGAGAACTTACG-3' and reverse 5'-CTGTAACTTCGACCAACACCTTTAAA-3'), *DROSHA* (forward 5'-GAACAGTTCAACCCCGATGTG-3' and reverse 5'-CTCAACTGTGCAGGGCGTATC-3'), *DGCR8* (forward 5'-TCTGCTCCTTAGCCCTGTCAGT-3' and reverse 5'-CCAACACTCCCGCCAAAG-3'), *EIF2C2* (forward 5'-GCACGGAAGTCCATCTGAAGTC-3' and reverse 5'-CCGGCGTCTCTCGAGATCT-3'), human 18S rRNA (forward 5'-CGCAGCTAGGAATAATGGAATAGG-3' and reverse 5'-GCCTCAGTTCCGAAAACCAA-3'), *Alu* (forward 5'-CAACATAGTGAAACCCCGTCTCT-3' and reverse 5'-GCCTCAGCCTCCCGAGTAG-3'), LINE *L1.3* (ORF2) (forward 5'-CGGTGATTTCTGCATTTCCA-3' and reverse 5'-TGTCTGGCACTCCCTAGTGAGA-3'), *HERV-WE1* (forward 5'- GCCGCTGTATGACCAGTAGCT-3' and reverse 5'-GGGACGCTGCATTCTCCAT-3'), human Ro-associated Y3 (*hY3*) (forward 5'-CCGAGTGCAGTGGTGTTTACA-3' and reverse 5'-GGAGTGGAGAAGGAACAAAGAAATC-3'), 7SL (forward 5'-CGGCATCAATATGGTGACCT-3' and reverse 5'-CTGATCAGCACGGGAGTTTT-3'), B1 (forward 5'-TGCCTTTAATCCCAGCACTT-3' and reverse 5'-GCTGCTCACACAAGGTTGAA-3'), B2 (forward 5'-GAGTTCAAATCCCAGCAACCA-3' and reverse 5'-AAGAGGGTCTCAGATCTTGTTACAGA-3'), *Dicer1* (forward 5'-CCCACCGAGGTGCATGTT-3' and reverse 5'-TAGTGGTAGGAGGCGTGTGTAAAA-3'), mouse 18S rRNA (forward 5'- TTCGTATTGCGCCGCTAGA-3' and reverse 5'-CTTTCGCTCTGGTCCGTCTT-3') were used. The QPCR cycling conditions were 50 °C for 2 min, 95 °C for 10 min followed by 40 cycles of a two-step amplification program (95 °C

for 15 s and 58 °C for 1 min). At the end of the amplification, melting curve analysis was applied using the dissociation protocol from the Sequence Detection system to exclude contamination with unspecific PCR products. The PCR products were also confirmed by agarose gel and showed only one specific band of the predicted size. For negative controls, no RT products were used as templates in the QPCR and verified by the absence of gel-detected bands. Relative expressions of target genes were determined by the $2^{-\Delta\Delta Ct}$ method.

**miRNA PCR.** miRNA abundance was quantified using the All-in-One™ miRNA qRT-PCR Detection Kit (GeneCopoeia). Briefly, total RNA was polyadenylated and reverse transcribed using a poly dT-adaptor primer. Quantitative RT-PCR was carried out using a miRNA-specific forward primer and universal reverse primer. PCR products were subjected to dissociation curve and gel electrophoresis analyses to ensure that single, mature miRNA products were amplified. Data were normalized to *ACTB* levels. The forward primers for the miRNAs were as follows: miR-184 (5'-TGGACGGAGAACTGATAAGGGT-3'); miR-221/222 (5'-AGCTACATCTGGCTACTGGGT-3'); miR-204/211 (5'-TTCCCTTTGTCATCCTTCGCCT-3'); miR-877 (5'-GTAGAGGAGATGGCGCAGGG-3'); miR-320a (5'-AAAAGCTGGGTTGAGAGGGCGA-3'); miR-484 (5'-TCAGGCTCAGTCCCCTCCCGAT-3'); let-7a (5'-TGAGGTAGTAGGTTGTATAGTT-3'). The reverse primers were proprietary (Genecopoeia). The primers for *ACTB* were forward (5'-TGGATCAGCAAGCAGGAGTATG-3') and reverse (5'-GCATTTGCGGTGGACGAT-3').

**Dot Blot (Immuno-Dot binding).** Increasing amounts of *Alu* RNA were spotted onto hybond-$N^+$ positively charged nylon membrane (Amersham) and UV cross-linked. After blocking, the membranes were incubated with mouse antibody against dsRNA (1:1,000,

clone J2) for 1 h at RT. The peroxidase-conjugated goat anti-mouse secondary antibody (1:5,000, Sigma) was used for 1 h at RT. After several washes, the signals were visualized by enhanced chemiluminescence (ECL plus, Amersham). *In vitro* transcribed dsRNAs of different length were used as positive controls. Transfer and ribosomal RNAs were used as negative controls.

**Northern Blot.** Total RNA from normal and diseased macular RPE was extracted as described above using Trizol. RNA integrity and quality was assessed using 1% agarose gel electrophoresis and RNA concentrations and purity were determined for each sample by NanoDrop 1000 spectrophotometer V3.7 (Thermo Fisher Scientific). dsRNA (2 µg) was separated on denaturing 15% PAGE-urea ready gel (Bio-Rad), and total RNA (10 µg) was separated by size on 1% agarose, 0.7M formaldehyde gels and visualized on an ultraviolet transilluminator to ensure consistent loading between different groups and to record the distance of migration of the 18S and 28S rRNA bands. dsRNA ladder (21–500 bp, New England BioLabs) and RNA ladder (0.1–2 kb, Invitrogen) were used as markers. Gels were then transferred to a positively charged Nylon membrane (Hybond-N+, GE Healthcare Bio-Sciences) by vacuum blotting apparatus (VacuGene XL Vacuum Blotting System, GE Healthcare Bio-Sciences). The RNAs were crosslinked to the membranes by ultraviolet irradiation and baked at 80 °C for 20–30 min. Membranes were hybridized with ($\alpha$-$^{32}$P)-dCTP-labeled DNA *Alu* probe at 42 °C overnight. On the following day, the membranes were rinsed twice with 1xSSC, 0.1% SDS at 55 °C. Each wash was for 20 min, and then membranes were subjected to storage in a phosphor autoradiography cassette. Hybridization signals were determined by using Typhoon phosphorimager (GE Healthcare Bio-Sciences). The 7SL probe was synthesized by PCR amplification of a 7SL RNA plasmid[29,36] with the

following primers (forward 5'- ATCGGGTGTCCGCACTAAG-3' and reverse 5'-ATCAGCACGGGAGTTTTGAC-3') designed to amplify a 128-bp fragment within the S-region that is not contained in *Alu*. For visualization of U6, membranes were stripped and blotted again using the High Sensitive MiRNA Northern Blot Assay Kit (Signosis) according to the manufacturer's instructions.

**Western Blot.** Tissues were homogenized in lysis buffer (10 mM Tris base, pH 7.4, 150 mM NaCl, 1 mM EDTA, 1 mM EGTA, 1% Triton X-100, 0.5% NP-40, protease and phosphatase inhibitor cocktail (Roche)). Protein concentrations were determined using a Bradford assay kit (Bio-Rad) with bovine serum albumin as a standard. Proteins (40–100 μg) were run on 4–12% Novex Bis-Tris gels (Invitrogen). The transferred membranes were blocked for 1 h at RT and incubated with antibodies against DICER1 (1:1,000, ref. 37; or 1:200, Santa Cruz Biotechnology) at 4 ºC overnight. Protein loading was assessed by immunoblotting using an anti-Tubulin antibody (1:1,000; Sigma-Aldrich). The secondary antibodies were used (1:5,000) for 1 h at RT. The signal was visualized by enhanced chemiluminescence (ECL Plus) and captured by VisionWorksLS Image Acquisition and Analysis software (Version 6.7.2, UVP, LLC). Densitometry analysis was performed using ImageJ (NIH). The value of 1 was arbitrarily assigned for normal eye samples.

**DICER1 cleavage.** The ability of DICER1 to cleave *Alu* RNA was tested using Recombinant Human Dicer Enzyme Kit (Genlantis) according the manufacturer's instructions. The products of the digestion were purified for the *in vivo* injection using RNA Purification Column (Genlantis).

**Cell culture.** All cell lines were cultured at 37 °C and 5% $CO_2$. Primary mouse RPE cells were isolated as previously described[38] and grown in Dulbecco Modified Eagle Medium

(DMEM) supplemented with 10% FBS and standard antibiotics concentrations. Primary human RPE cells were isolated as previously described[39] and maintained in DMEM supplemented with 20% FBS and antibiotics. Parental HCT116 and isogenic Dicer$^{ex5}$ cells[1] were cultured in McCoy's 5A medium supplemented with 10% FBS.

**Transient transfection.** Human and mouse RPE cells were transfected with pUC19, pAlu, pCDNA3.1/Dicer1-FLAG, pCDNA3.1, DICER1 antisense oligonucleotide (as) (5'-GCUGACCTTTTTGCTUCUCA-3'), B1/B2 as (5'-TCAGATCTCGTTACGGATGGTTGTGA-3'), control (for DICER1 and B1/B2) as (5'-TTGGTACGCATACGTGTTGACTGTGA-3'), *Alu* as (5'-CCCGGGTTCACGCCATTCTCCTGCCTCAGCCTCACGAGTAGCTGGGACTACAGGCGCCCGACACCACTCCCGGCTAATTTTTTGTATTTTT-3'), control (for *Alu*) as (5'-GCATGGCCAGTCCATTGATCTTGCACGCTTGCCTAGTACGCTCCTCAACCTATCCTCCTAGCCCGTTACTTGGTGCCACCGGCG-3') using Lipofectamine 2000 (Invitrogen) or Oligofectamine (Invitrogen) according to the manufacturer's instructions.

**Adenoviral infection.** Cells were plated at density of $15\times10^3/cm^2$ and after 16 h, at approximately 50% confluence, were infected with AdCre or AdNull (Vector Laboratories) with a multiplicity of infection of 1,000.

**RNA polymerase inhibition.** Human RPE cells were transfected with DICER1 or control antisense oligonucleotides using Lipofectamine 2000. After a change of medium at 6 h, the cells were incubated with 45 μM tagetitoxin (Epicentre Technologies, Tagetin) or 10 μg/ml a-amanitin (Sigma-Aldrich) and the total RNA was collected after 24 h.

**Cell viability.** MTS assays were performed using the CellTiter 96 AQueous One Solution Cell Proliferation Assay (Promega) in according to the manufacturer's instructions.

**Caspase-3 activity.** Sub-confluent human RPE cells were treated with PBS or *Alu* RNA at different concentrations in 2% FBS medium for 8 h. The caspase-3 activity was measured using Caspase-3 Fluorimetric Assay (R&D Systems) according to the manufacturer's instructions.

**Oxidative stress.** Confluent human RPE cells were exposed to hydrogen peroxide (0–2 mM, Fisher Scientific).

**Statistics.** Results are expressed as mean ± SEM, with $P<0.05$ considered statistically significant. Differences between groups were compared by using Mann–Whitney U test or Student t test, as appropriate, and 2-tailed *P* values are reported.

**Supplemental References**


1. Cummins, J. M. *et al.* The colorectal microRNAome. *Proc Natl Acad Sci U S A* **103**, 3687-3692 (2006).
2. Batzer, M. A. & Deininger, P. L. Alu repeats and human genomic diversity. *Nat Rev Genet* **3**, 370-379 (2002).
3. Shaikh, T. H., Roy, A. M., Kim, J., Batzer, M. A. & Deininger, P. L. cDNAs derived from primary and small cytoplasmic Alu (scAlu) transcripts. *J Mol Biol* **271**, 222-234 (1997).
4. Sinnett, D., Richer, C., Deragon, J. M. & Labuda, D. Alu RNA transcripts in human embryonal carcinoma cells. Model of post-transcriptional selection of master sequences. *J Mol Biol* **226**, 689-706 (1992).

5. Rattner, A., Toulabi, L., Williams, J., Yu, H. & Nathans, J. The genomic response of the retinal pigment epithelium to light damage and retinal detachment. *J Neurosci* **28**, 9880-9889 (2008).

6. Huang, H. *et al.* Identification of mouse retinal genes differentially regulated by dim and bright cyclic light rearing. *Exp Eye Res* **80**, 727-739 (2005).

7. Natoli, R., Provis, J., Valter, K. & Stone, J. Gene regulation induced in the C57BL/6J mouse retina by hyperoxia: a temporal microarray study. *Mol Vis* **14**, 1983-1994 (2008).

8. Farjo, R., Peterson, W. M. & Naash, M. I. Expression profiling after retinal detachment and reattachment: a possible role for aquaporin-0. *Invest Ophthalmol Vis Sci* **49**, 511-521 (2008).

9. Livesey, F. J., Furukawa, T., Steffen, M. A., Church, G. M. & Cepko, C. L. Microarray analysis of the transcriptional network controlled by the photoreceptor homeobox gene Crx. *Curr Biol* **10**, 301-310 (2000).

10. Gehrig, A. *et al.* Genome-wide expression profiling of the retinoschisin-deficient retina in early postnatal mouse development. *Invest Ophthalmol Vis Sci* **48**, 891-900 (2007).

11. Hackam, A. S. *et al.* Identification of gene expression changes associated with the progression of retinal degeneration in the rd1 mouse. *Invest Ophthalmol Vis Sci* **45**, 2929-2942 (2004).

12. Punzo, C. & Cepko, C. Cellular responses to photoreceptor death in the rd1 mouse model of retinal degeneration. *Invest Ophthalmol Vis Sci* **48**, 849-857 (2007).

13. Schaeferhoff, K. *et al.* Induction of STAT3-related genes in fast degenerating cone photoreceptors of cpfl1 mice. *Cell Mol Life Sci* **67**, 3173-3186 (2010).

14. Gelineau-van Waes, J. *et al.* Altered expression of the iron transporter Nramp1 (Slc11a1) during fetal development of the retinal pigment epithelium in microphthalmia-associated transcription factor Mitf(mi) and Mitf(vitiligo) mouse mutants. *Exp Eye Res* **86**, 419-433 (2008).

15. Tian, J. *et al.* Advanced glycation endproduct-induced aging of the retinal pigment epithelium and choroid: a comprehensive transcriptional response. *Proc Natl Acad Sci U S A* **102**, 11846-11851 (2005).

16. Zacks, D. N., Han, Y., Zeng, Y. & Swaroop, A. Activation of signaling pathways and stress-response genes in an experimental model of retinal detachment. *Invest Ophthalmol Vis Sci* **47**, 1691-1695 (2006).

17. Chong, M. M., Rasmussen, J. P., Rudensky, A. Y. & Littman, D. R. The RNAseIII enzyme Drosha is critical in T cells for preventing lethal inflammatory disease. *J Exp Med* **205**, 2005-2017 (2008).

18. Iacovelli, J. *et al.* Generation of cre transgenic mice with postnatal RPE-specific ocular expression. *Invest Ophthalmol Vis Sci*, In press (2010).

19. Yi, R. *et al.* DGCR8-dependent microRNA biogenesis is essential for skin development. *Proc Natl Acad Sci U S A* **106**, 498-502 (2009).

20. Zhong, J., Peters, A. H., Lee, K. & Braun, R. E. A double-stranded RNA binding protein required for activation of repressed messages in mammalian germ cells. *Nat Genet* **22**, 171-174 (1999).

21. Ambati, J. *et al.* An animal model of age-related macular degeneration in senescent Ccl-2- or Ccr-2-deficient mice. *Nat Med* **9**, 1390-1397 (2003).

22. Takeda, A. *et al.* CCR3 is a target for age-related macular degeneration diagnosis and therapy. *Nature* **460**, 225-230 (2009).

23. Hahn, P. *et al.* Disruption of ceruloplasmin and hephaestin in mice causes retinal iron overload and retinal degeneration with features of age-related macular degeneration. *Proc Natl Acad Sci U S A* **101**, 13850-13855 (2004).

24. O'Carroll, D. *et al.* A Slicer-independent role for Argonaute 2 in hematopoiesis and the microRNA pathway. *Genes Dev* **21**, 1999-2004 (2007).

25. Schaefer, A. *et al.* Argonaute 2 in dopamine 2 receptor-expressing neurons regulates cocaine addiction. *J Exp Med* **207**, 1843-1851 (2010).

26. Provost, P. *et al.* Ribonuclease activity and RNA binding of recombinant human Dicer. *EMBO J* **21**, 5864-5874 (2002).

27. Bennett, E. A. *et al.* Active Alu retrotransposons in the human genome. *Genome Res* **18**, 1875-1883 (2008).

28. Hagan, C. R., Sheffield, R. F. & Rudin, C. M. Human Alu element retrotransposition induced by genotoxic stress. *Nat Genet* **35**, 219-220 (2003).

29. Misra, S., Tripathi, M. K. & Chaudhuri, G. Down-regulation of 7SL RNA expression and impairment of vesicular protein transport pathways by Leishmania infection of macrophages. *J Biol Chem* **280**, 29364-29373 (2005).

30. Alexander, J. J. & Hauswirth, W. W. Adeno-associated viral vectors and the retina. *Adv Exp Med Biol* **613**, 121-128 (2008).

31. Maan, S. *et al.* Rapid cDNA synthesis and sequencing techniques for the genetic study of bluetongue and other dsRNA viruses. *J Virol Methods* **143**, 132-139 (2007).

32. Potgieter, A. C. *et al.* Improved strategies for sequence-independent amplification and sequencing of viral double-stranded RNA genomes. *J Gen Virol* **90**, 1423-1432 (2009).

33. Kohany, O., Gentles, A. J., Hankus, L. & Jurka, J. Annotation, submission and screening of repetitive elements in Repbase: RepbaseSubmitter and Censor. *BMC Bioinformatics* **7**, 474 (2006).

34. Altschul, S. F., Gish, W., Miller, W., Myers, E. W. & Lipman, D. J. Basic local alignment search tool. *J Mol Biol* **215**, 403-410 (1990).

35. Allen, T. A., Von Kaenel, S., Goodrich, J. A. & Kugel, J. F. The SINE-encoded mouse B2 RNA represses mRNA transcription in response to heat shock. *Nat Struct Mol Biol* **11**, 816-821 (2004).

36. Tripathi, M. K. & Chaudhuri, G. Down-regulation of UCRP and UBE2L6 in BRCA2 knocked-down human breast cells. *Biochem Biophys Res Commun* **328**, 43-48 (2005).

37. Kanellopoulou, C. *et al.* Dicer-deficient mouse embryonic stem cells are defective in differentiation and centromeric silencing. *Genes Dev* **19**, 489-501 (2005).

38. Yang, P., Tyrrell, J., Han, I. & Jaffe, G. J. Expression and modulation of RPE cell membrane complement regulatory proteins. *Invest Ophthalmol Vis Sci* **50**, 3473-3481 (2009).

39. Yang, Z. *et al.* Toll-like receptor 3 and geographic atrophy in age-related macular degeneration. *N Engl J Med* **359**, 1456-1463 (2008).